RNase protection assay. For the specific analysis of the PPAR-γ3 relative to PPAR-γ1 mRNA, we constructed a template for probe synthesis using an RT-PCR product derived from mouse adipose tissue RNA with oligonucleotides that bind sense at exon A1 and antisense at exon 2. The amplified fragment was inserted blunt into pCR2.1 (TA cloning, Invitrogen). The resulting plasmid pCR2.1–PPAR-γ3–RPA, which contains part of exon A1, the full-length exon A2, exon 1 and part of exon 2, was used as a template for probe synthesis. To analyse PPAR-γ2 and PPAR-γ1, the coding region from +1 to +284 was obtained as an RT-PCR product from mouse adipose tissue RNA and cloned into pCR2.1, then subcloned into pBluescript KS+ (Stratagene). We used the resulting plasmid as a template for synthesis of the antisense RNA probe, allowing detection of PPAR-γ2 and PPAR-γ1 mRNA. The common PPAR-γ probe corresponding to nucleotides 800–1093 of the murine cDNA was subcloned into pBluescript SK+ (Stratagene). RNase protection experiments were done as described[12]. Resident peritoneal macrophages were treated in the presence or absence of IL-4 for 18 h. We used a β-actin antisense probe to verify equivalent amounts of total mRNA.

Received 28 April; accepted 20 May 1999.

1. Tontonoz, P., Hu, E. & Spiegelman, B. M. Stimulation of adipogenesis in fibroblasts by PPARγ2, a lipid-activated transcription factor. *Cell* **79,** 1147–1156 (1994).
2. Lehmann, J. M. *et al.* An antidiabetic thiazolidinedione is a high affinity ligand for peroxisome proliferator-activated receptor-γ (PPARγ). *J. Biol. Chem.* **270,** 12953–12956 (1995).
3. Willson, T. M. *et al.* The structure–activity relationship between peroxisome proliferator-activated receptor γ agonism and the antihyperglycemic activity of thiazolidinediones. *J. Med. Chem.* **39,** 665–668 (1996).
4. Tontonoz, P., Nagy, L., Alvarez, J. G. A., Thomazy, V. A. & Evans, R. M. PPARγ promotes monocyte/macrophage differentiation and uptake of oxidized LDL. *Cell* **93,** 241–252 (1998).
5. Ricote, M., Li, A. C., Willson, T. M., Kelly, C. J. & Glass, C. K. The peroxisome proliferator-activated receptor-γ is a negative regulator of macrophage activation. *Nature* **391,** 79–82 (1998).
6. Jiang, C., Ting, A. T. & Seed, B. PPAR-γ agonists inhibit production of monocyte inflammatory cytokines. *Nature* **391,** 82–86 (1998).
7. Kliewer, S. A. *et al.* Fatty acids and eicosanoids regulate gene expression through direct interactions with peroxisome proliferator-activated receptors α and γ. *Proc. Natl Acad. Sci. USA* **94,** 4318–4323 (1997).
8. Kliewer, S. A. *et al.* A prostaglandin J_2 metabolite binds peroxisome prolifator-activated receptorγ and promotes adipocyte differentiation. *Cell* **83,** 813–819 (1995).
9. Forman, B. M. *et al.* 15-Deoxy-$\Delta^{12,14}$-prostaglandin J_2 is a ligand for the adipocyte determination factor PPARγ. *Cell* **83,** 803–812 (1995).
10. Nagy, L., Tontonoz, P., Alvarez, J. G. A., Chen, H. & Evans, R. M. Oxidized LDL regulates macrophage gene expression through ligand activation of PPAR-γ. *Cell* **93,** 229–240 (1998).
11. Conrad, D. J., Kuhn, H., Mulkins, M., Highland, E. & Sigal, E. Specific inflammatory cytokines regulate the expression of human monocyte 15-lipoxygenase. *Proc. Natl Acad. Sci. USA* **89,** 217–221 (1992).
12. Ricote, M. *et al.* Expression of the peroxisome proliferator-activated receptor γ (PPARγ) in human atherosclerosis and regulation in macrophages by colony stimulating factors and oxidized low density lipoprotein. *Proc. Natl Acad. Sci. USA* **95,** 7614–7619 (1998).
13. Zhu, Y. *et al.* Structural organization of mouse peroxisome proliferator-activated receptor γ (mPPAR γ) gene: alternative promoter use and different splicing yield two mPPAR γ isoforms. *Proc. Natl Acad. Sci. USA* **92,** 7921–7925 (1995).
14. Fajas, L., Fruchart, J. C. & Auwerx, J. PPARγ3 mRNA: a distinct PPARγ mRNA subtype transcribed from an independent promoter. *FEBS Lett.* **438,** 55–60 (1998).
15. Yamamoto, S. Mammalian lipoxygenases: molecular structure and functions. *Biochem. Biophys. Res. Commun.* **1128,** 117–131 (1992).
16. van Leyen, K., Duvoisin, R. M., Engelhardt, H. & Wiedmann, M. A function for lipoxygenase in programmed organelle degradation. *Nature* **395,** 392–395 (1998).
17. Rankin, S. M., Parthasarathy, S. & Steinberg, D. Evidence for a dominant role of lipoxygenase(s) in the oxidation of LDL by mouse peritoneal macrophages. *J. Lipid Res.* **32,** 449–456 (1991).
18. Benz, D. J. *et al.* Enhanced levels of lipoperoxides in low density lipoproteins incubated with murine fibroblasts expressing high levels of human 15-lipoxygenase. *J. Biol. Chem.* **270,** 5191–5197 (1995).
19. Funk, C. D. The molecular biology of mammalian lipoxygenases and the quest for eicosanoid functions using lipoxygenase-deficient mice. *Biochim. Biophys. Acta* **1304,** 65–84 (1996).
20. Kuhn, H. Biosynthesis, metabolization and biological importance of the primary 15-lipoxygenase metabolites 15-hydro(pero)xy-5Z,8Z,11Z,13E-eicosatetraenoic acid and 13-hydro(pero)xy-9Z,11E-octadecadienoic acid. *Prog. Lipid Res.* **35,** 203–226 (1996).
21. Heydeck, D. *et al.* Interleukin-4 and -13 induce upregulation of the murine macrophage 12/15-lipoxygenase activity: evidence for the involvement of transcription factor STAT6. *Blood* **92,** 2503–2510 (1998).
22. Scheidegger, K. J., Butler, S. & Witztum, J. L. Angiotensin II increases macrophage-mediated modification of low density lipoprotein via a lipoxygenase-dependent pathway. *J. Biol. Chem.* **272,** 21609–21615 (1997).
23. Bogdan, C., Vodovotz, Y., Paik, J., Xie, Q.-W. & Nathan, C. Mechanism of suppression of nitric oxide synthase expression by interleukin-4 in primary mouse macrophages. *J. Leukocyte Biol.* **55,** 227–233 (1994).
24. Yesner, L. M., Huh, H. Y., Pearce, S. F. & Silverstein, R. L. Regulation of monocyte CD36 and thrombospondin-1 expression by soluble mediators. *Arterioscler. Thromb. Vasc. Biol.* **16,** 1019–1025 (1996).
25. Yamada, Y., Doi, T., Hamakubo, T. & Kodama, T. Scavenger receptor family proteins: roles for atherosclerosis, host defence and disorders of the central nervous system. *Cell. Mol. Life Sci.* **54,** 628–640 (1998).
26. Endemann, G. *et al.* CD36 is a receptor for oxidized low density lipoprotein. *J. Biol. Chem.* **268,** 11811–11816 (1993).
27. Savill, J. S., Hogg, N., Ren, Y. & Haslett, C. Thrombospondin cooperates with CD36 and the vitronectin receptor in macrophage recognition of neutrophils undergoing apoptosis. *J. Clin. Invest.* **90,** 1513–1522 (1992).
28. Sun, D. & Funk, C. D. Disruption of 12/15-lipoxygenase expression in peritoneal macrophages. *J. Biol. Chem.* **271,** 24055–24062 (1996).
29. Nolte, R. T. *et al.* Ligand binding and co-activator assembly of the peroxisome proliferator-activated receptor-γ. *Nature* **395,** 137–143 (1998).
30. Sigal, E. C., Craik, C. S. & Highland, E. Molecular cloning and primary structure of human 15-lipoxygenase. *Biochem. Biophys. Res. Commun.* **157,** 457–464 (1988).

Acknowledgements. We thank S. Blanchard (Glaxo Wellcome) for communicating results of the characterization of GW9662 before publication; T. Schneiderman for assistance with manuscript preparation; and J. Barnett for assistance in preparation of human peripheral blood monocytes. J.T.H. is supported by an NIH Postdoctoral Fellowship. J.S.W. is supported by an NIH Medical Scientist Training Program Grant to U. C. San Diego. M.R. is supported by a Postdoctoral Fellowship from the American Heart Association. C.J.K. and D.C. are clinical investigators of the Medical Research Service, Department of Veterans Affairs. C.K.G. is an Established Investigator of the American Heart Association. These studies were also supported by NIH grants to C.D.F. and C.K.G. and a Specialized Center of Research Grant in Atherosclerosis to J.L.W. and C.K.G.

Correspondence and requests for materials should be addressed to C.K.G. (e-mail: cglass@ucsd.edu).

Regulation of cell movement is mediated by stretch-activated calcium channels

Juliet Lee*†, Akira Ishihara*, Gerry Oxford‡, Barry Johnson§ & Ken Jacobson*‖

** Department of Cell Biology and Anatomy, ‖ Lineberger Comprehensive Cancer Center and ‡ Department of Molecular and Cell Physiology, University of North Carolina, Chapel Hill, North Carolina 27599-7090, USA*
§ Department of Physiology and Neurobiology, University of Connecticut, 75 North Eagleville Road, U-156, Storrs, Connecticut 06269, USA

Intracellular calcium regulates many of the molecular processes that are essential for cell movement[1]. It is required for the production of actomyosin-based contractile forces[2–4], the regulation of the structure and dynamics of the actin cytoskeleton[5,6], and the formation and disassembly of cell–substratum adhesions[7,8]. Calcium also serves as a second messenger in many biochemical signal-transduction pathways[7]. However, despite the pivotal role of calcium in motile processes, it is not clear how calcium regulates overall cell movement. Here we show that transient increases in intracellular calcium, $[Ca^{2+}]_i$, during the locomotion of fish epithelial keratocytes, occur more frequently in cells that become temporarily 'stuck' to the substratum or when subjected to mechanical stretching. We find that calcium transients arise from the activation of stretch-activated calcium channels, which triggers an influx of extracellular calcium. In addition, the subsequent increase in $[Ca^{2+}]_i$ is involved in detachment of the rear cell margin. Thus, we have defined a mechanism by which cells can detect and transduce mechanical forces into biochemical signals that can modulate locomotion.

The simple shape and rapid locomotion of fish keratocytes makes them an excellent system in which to study cell movement. These features have been exploited in several studies that have provided insight into how cytoskeletal dynamics, adhesion formation and force generation are integrated to produce movement[9–15]. Most of this work has focused on fan-shaped keratocytes that exhibit a rapid 'gliding' mode of movement. However, these cells can also exhibit a much slower mode of movement closely resembling that of fibroblasts, in which extension of the front edge of the cell occurs as a distinct phase from retraction of the rear edge. Individual keratocytes can also switch between these two modes of movement, which is a particularly useful characteristic for studying how cell movement is regulated.

To investigate the role of calcium in the regulation of keratocyte locomotion, we used fluorescence video microscopy to continuously monitor $[Ca^{2+}]_i$ in moving keratocytes (Fig. 1a, b). The resting level of $[Ca^{2+}]_i$ was found to be ~138 nM. However,

† Present address: Department of Molecular and Cell Biology, University of Connecticut, 75 North Eagleville Road, U-125, Storrs, Connecticut 06269, USA.

keratocytes exhibited transient increases in $[Ca^{2+}]_i$ (Fig. 1c–h) ranging from 219 to 683 nM, corresponding to an increase of between 160 and 500% in fluorescence intensity of the calcium indicator above the baseline value (Fig. 1i). Dual fluorescence imaging of a calcium-insensitive rhodamine dextran and Calcium Green I dextran that were previously co-loaded into keratocytes confirmed that fluctuations in cell thickness were not contributing to changes in brightness of the calcium indicator (Fig. 1j). The frequency, duration and relative magnitude of calcium transients was compared between fan-shaped cells that exhibited a rapid,

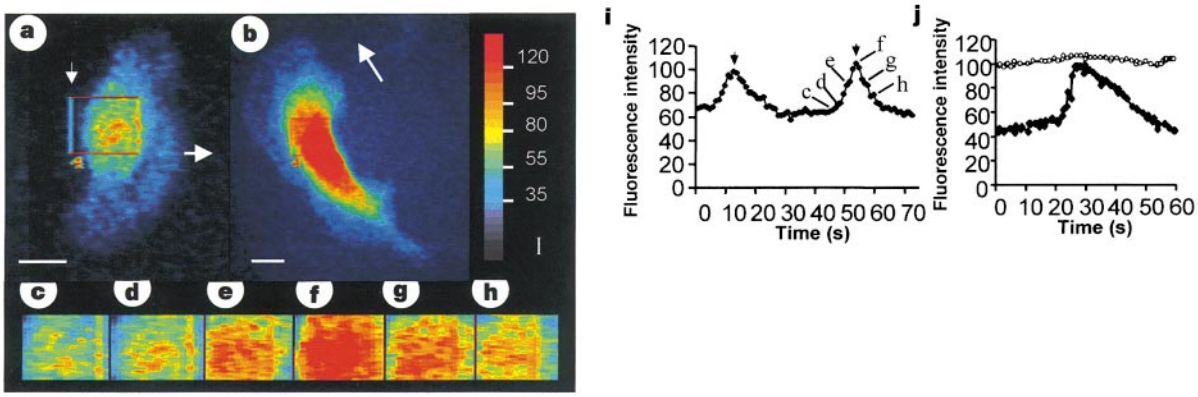

Figure 1 Calcium transients occur in moving keratocytes. **a**, **b**, Pseudocoloured (non-ratiometric) fluorescence images of a fan-shaped keratocyte (**a**) and a fibroblastic-shaped keratocyte (**b**), moving as indicated (arrows). The colour key represents fluorescence intensity (*I*) in grey level units. **c**–**h**, A series of square regions taken every 4 s from the cell in **a** showing a transient increase in $[Ca^{2+}]_i$ as a brief increase in red colour. **i**, Plot of average fluorescence intensity over time within the same region with points corresponding to regions (**c**–**h**) marked (on the second transient, arrow). The same relative increase in fluorescence occurs throughout the cell, but the nuclear region appears brighter because it is thicker. However, differences in cell thickness do not affect the observation of transients. **j**, Plot of the fluorescence intensity from a calcium-insensitive rhodamine dextran (circles) shows no change compared with the transient increase in fluorescence from the calcium indicator (squares). Scale bars, 10 μm.

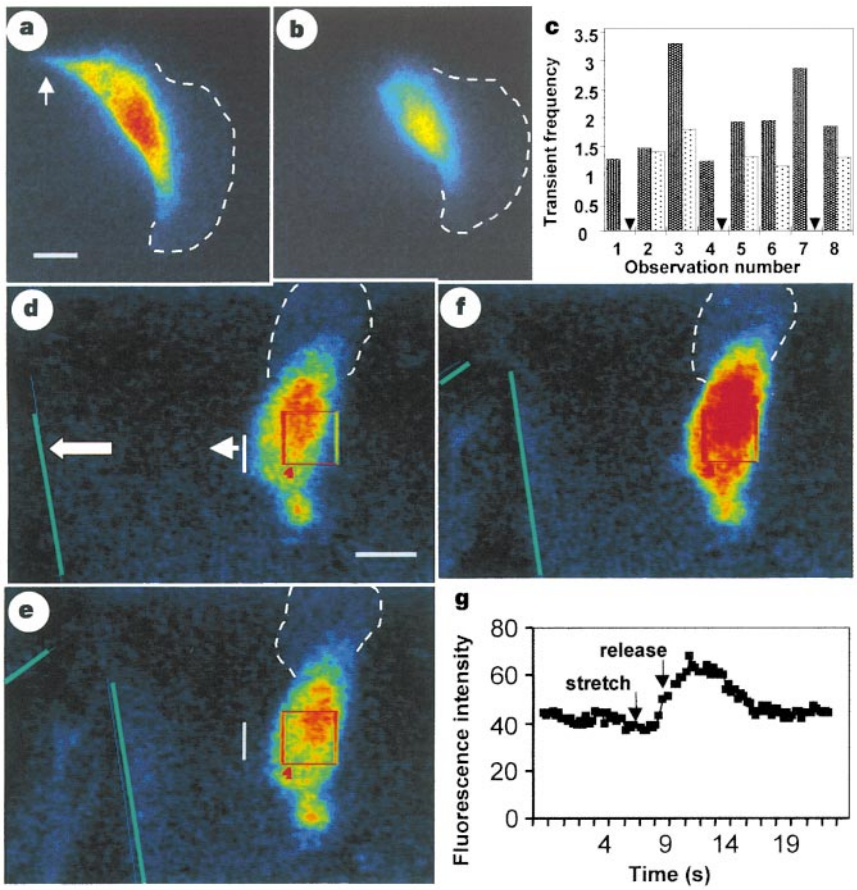

Figure 2 Increases in $[Ca^{2+}]_i$ in response to stretching. **a**, A stretched keratocyte with a 'tether' (arrow). **b**, The same cell following detachment (dashed line represents front cell edge). **c**, Transient frequency (per minute) or zero transients (triangles) in tethered cells (dark bars) and after detachment (pale bars). **d**, A microneedle (green line) is used to deform an elastic substratum in the direction indicated (arrow). The cell is stretched for ~2 s in the same direction (white vertical bar). **e**, The microneedle and the cell return to their pre-stretch positions. Note the position of the cell body with respect to its stretched position (white bar). **f**, The calcium transient induced in response to stretching is shown as an increase in red over the cell body. **g**, Plot of fluorescence intensity versus time, showing that a calcium transient is induced about 1 s after stretch initiation. Scale bar, 10 μm.

gliding mode of locomotion and fibroblastic-shaped cells that exhibited a slow, discontinuous mode of movement. Calcium transients were found to occur about three times more frequently in fibroblastic-shaped keratocytes (mean 1.69 per min, s.e.m. 0.33, $n = 25$) than in fan-shaped cells (mean 0.62 per min, s.e.m. 0.22, $n = 12$). Most fan-shaped keratocytes did not exhibit any transients within an observation period of 2–3 min, whereas most fibroblastic-shaped cells displayed three transients a minute, and sometimes as many as six. No significant difference was found in the duration or magnitude of the transients displayed by these subgroups of keratocytes.

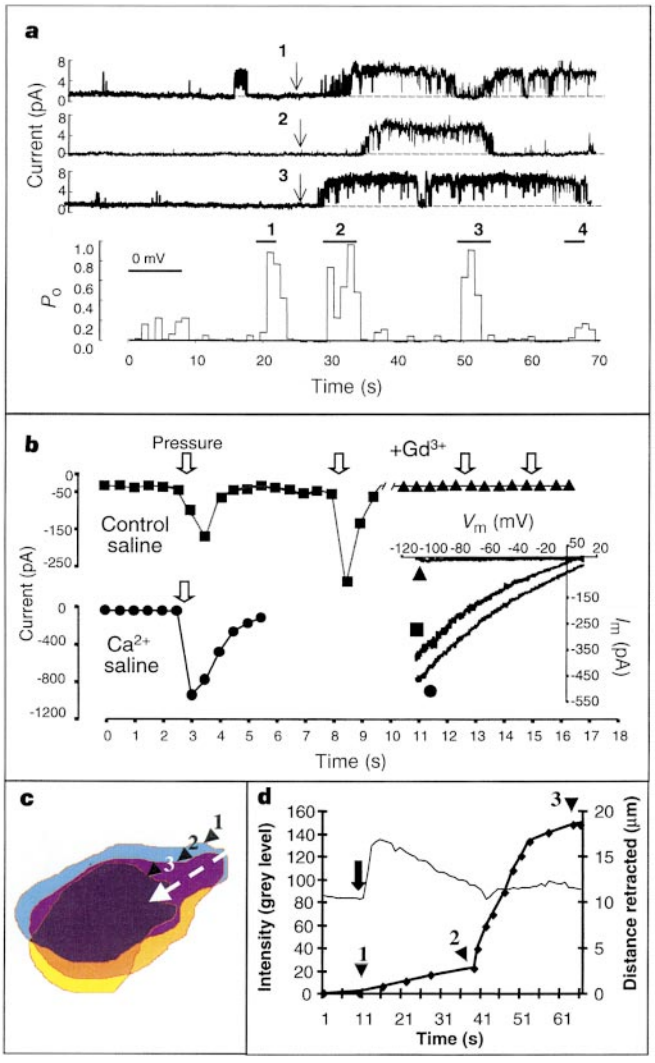

Figure 3 Direct evidence for stretch-activated calcium channels. **a**, Activity of a single stretch-activated channel plotted (traces) for three recording periods of 4 s each centred on the application of negative pressure (arrows 1, 2, 3). Activity of the channels increases markedly each time. The graph (bottom) is a continuous display of the open probability (P_o) for this channel binned into 1 s epochs. Bars 1, 2, 3 and 4 represent the duration of suction. **b**, Stretch-activated channels in keratocytes conduct Ca^{2+} and are blocked by Gd^{3+}. Recordings from stretch-activated channels in the whole-cell patch-clamp configuration, in control saline (squares), Ca^{2+} saline (circles) and following addition of Gd^{3+} (triangles). Deflections in these graphs (open arrows) correspond to the activation of stretch-activated calcium channels after a brief 'puff' of pressure and represent an influx of cations (squares) or calcium (circles). Channel activity in control saline is completely blocked by 100 μM Gd^{3+} (triangles). Representative leak-subtracted channel current–voltage relations (inset) for each condition measured using voltage ramps during the application of pressure. **c**, **d**, Rear retraction induced by the photorelease of caged ionophore. **c**, Cell outlines (triangles 1–3) during retraction (along dashed line). **d**, A plot of calcium indicator fluorescence (plain line) and retraction rate (line with symbols; triangles correspond to outlines in **c**) shows that retraction is initiated (triangle 1) immediately after photoactivation (bold arrow) and the resultant increase in $[Ca^{2+}]_i$. Retraction proceeds slowly while $[Ca^{2+}]_i$ returns to its resting level and then proceeds rapidly to completion (triangles 2 and 3).

Calcium transients were abolished in medium containing low calcium concentrations, or by the addition of EGTA to the culture medium, indicating that extracellular calcium is required. Treatment with 50 μM verapamil, a voltage-gated calcium-channel inhibitor, led to a 38% ($n = 8$) irreversible reduction in transient frequency. A larger reduction (57%, $n = 12$) in transient frequency was observed following treatment with 10 μM gadolinium (Gd^{3+}), which is known to block stretch-activated calcium channels, indicating that an influx of extracellular calcium through these channels is involved. Gadolinium treatment also inhibited detachment of the rear cell margin, causing cells to become elongated and eventually to cease movement (data not shown). When cells were placed in a high-potassium buffer, the frequency of calcium transients was not increased, as might be expected if voltage-dependent channels were having a significant effect. Treatment of keratocytes with thapsigargin (1 μM), to deplete calcium from intracellular stores, completely inhibited calcium transients, indicating that these arise from a calcium-induced calcium release within the cell. Furthermore, the frequency of calcium transients was markedly reduced (83%, $n = 8$) by treatment with cytochalasin D (250 ng), consistent with a requirement for an intact actin cytoskeleton.

To investigate the role of calcium transients in locomotion, alterations in cell shape were monitored in relation to changes in $[Ca^{2+}]_i$. In fibroblastic-shaped cells (Fig. 2a), a clear increase in transient frequency was observed as cells become elongated, before the rear cell edge was retracted (Fig. 2b). This is particularly striking for 'tethered' cells, whose movement becomes impeded when a small portion of the cell margin is temporarily unable to detach from the substratum (Fig. 2a). The frequency of transients in tethered cells is greatly reduced following retraction (Fig. 2c). These results, together with the finding that transients could be inhibited by Gd^{3+}, point to the involvement of stretch-activated calcium channels.

To test this idea, experiments were performed to determine whether an externally applied mechanical force could induce calcium transients, by stretching keratocytes without direct physical contact. Cells preloaded with calcium indicator were plated onto elastic substrata and stretched using paired microneedles on either side of the cell to deform the underlying substratum (Fig. 2d–f). In most cases (22 out of 27), a transient increase in $[Ca^{2+}]_i$ could be induced immediately after stretching (Fig. 2g). Nine of these stretched cells responded to a second stretch stimulus, and only three of these responded to a third stretch, indicating that keratocytes can adapt to repeated stretch stimuli. The increase in fluorescence intensity associated with stretch-induced transients was not significantly different from ones that occur normally.

Direct evidence for the existence of stretch-activated channels in keratocytes was obtained from single-channel recordings within membrane-attached patches ($n = 7$; Fig. 3a) and from whole-cell patch-clamp experiments (Fig. 3b). During the single-channel recording, three consecutive stretching stimuli were given to a small region of the cell membrane by applying negative pressure to the patch electrode. This was followed immediately by a dramatic increase in channel activity (Fig. 3a, top three rows). The spontaneous channel activity is greater at a pipette voltage of 0 mV (horizontal bar) than at +50 mV (remainder of recording). This is consistent with previous observations that stretch-activated channel opening is more frequent with membrane depolarization[16]. In addition, the open probability (P_o) increases dramatically during application of negative pressure (bars 1, 2, 3) and decreases rapidly after re-establishing normal pressure, indicating that the recordings

are channel responses and not nonspecific behaviour, such as seal breakdown (Fig. 3a, bottom graph). Stretch activation could be induced consecutively three times with repeated applications of suction. Furthermore, this channel undergoes an adaptive response to the applied force. This was initially manifest by a decline in P_o despite continued suction (response 3), and finally by a markedly weakened response to a subsequent stimulus (response 4). Such adaptation of stretch-activated channel responses has previously been reported[17,18], and is consistent with reduced cellular responses to repeated stretches, as mentioned above. Finally, despite uncertainty of the absolute value of patch membrane potential (cell interior resting potential was not measured), we estimated the single-channel conductance from the difference in current amplitudes at pipette voltages of 0 and +50 mV. Calculations for four membrane patches yielded values of 51, 52, 55 and 56 pS, within the range of values previously measured for cation-selective stretch-activated channels[19].

Whole-cell patch experiments showed that stretch-activated channels (Fig. 3b) could be activated in response to the application of brief 'puffs' of pressure through the patch pipette. Measurement of stretch-activated channel currents in control extracellular saline were characterized by a current–voltage relation with slight inward rectification, a reversal potential (E_{rev}) of 5 ± 1 mV ($n = 7$) and a complete block by 100 μM Gd^{3+}. The activation of stretch-activated channels was shown to mediate an influx of extracellular calcium.

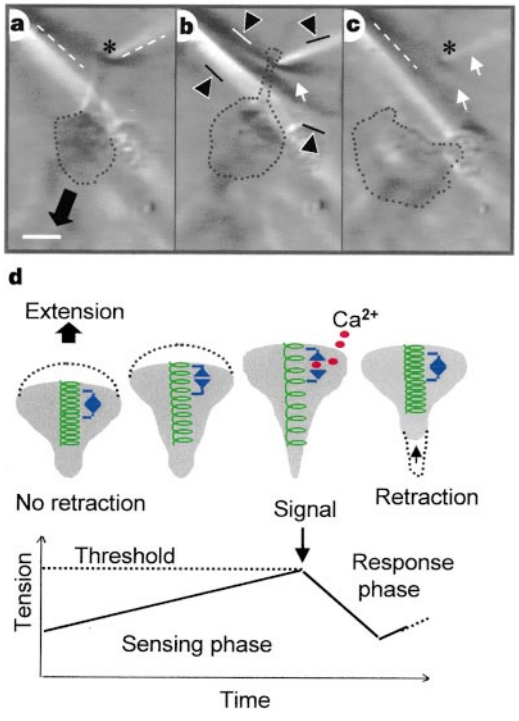

Figure 4 A scheme for the mechano-chemical regulation of movement. **a**–**c**, Phase-contrast images taken at 5-s intervals of a keratocyte on an elastic substratum. **a**, The front edge (dark dotted line) is extending (black arrow) but the rear (asterisk) is stuck. **b**, Increasing tension compresses the substratum between the regions indicated between opposing arrowheads, causing a new wrinkle to form (white arrow) and the pre-existing wrinkles (white dashed lines in **a**) to become more prominent. **c**, When retraction occurs (from the asterisk), tension is released so that two wrinkles disappear (white arrows) and the remaining wrinkle (white, dashed line) becomes less prominent. The cell now becomes fan shaped (dark dotted line). Scale bar, 10 μm. **d**, A tethered cell outline (grey) showing the cytoskeleton (green spiral) mechanically coupled to stretch-activated calcium channels (blue). During extension (dotted line), the cell is stretched and tension increases (graph). When a critical threshold is reached (dotted line), the calcium channels are activated, causing an influx of extracellular calcium (red) and a transient increase in $[Ca^{2+}]_i$, which induces rear retraction.

Thus, when Na^+ and K^+ in the extracellular saline were replaced with Ca^{2+}, the stretch-activated channel carried currents of the same density as the control (control, 67 ± 25 pA pF^{-1}, $n = 7$; Ca^{2+}, 61 ± 11 pA pF^{-1}, $n = 5$), demonstrating that these channels are capable of generating a significant intracellular Ca^{2+} signal. The reversal potential of these Ca^{2+} currents was shifted by +25 mV compared to control currents (E_{rev}, 30 ± 6 mV; $n = 5$), indicating that the channel is slightly more permeable to Ca^{2+} than to Na^+, when both are compared to Cs^+, which was the main internal cation in these experiments.

To investigate the role of increased $[Ca^{2+}]_i$ in the regulation of keratocyte movement, photoactivation of caged compounds was used to induce calcium transients, and the resulting alterations in cell shape were observed (Fig. 3c, d). Induction of a calcium transient could be achieved after the photorelease of either the caged ionophore A23187, which triggers an influx of extracellular calcium, or inositol 1,4,5-triphosphate, which induces Ca^{2+} release from intracellular stores. In both cases, induction of a calcium transient was usually followed by retraction of the rear cell margin (Fig. 3c). Retraction of the cell margin occurred preferentially at the rear of the cell, even though the relative magnitude of the $[Ca^{2+}]_i$ increase is the same throughout the cell. Retractions were not observed in control experiments in which cells were exposed to ultraviolet in the absence of caged compound.

Our experimental data, together with observations of tethered keratocytes on wrinkling silicone substrata (Fig. 4a–c), suggest the following scheme for the mechanochemical regulation of cell movement. When the rate of retraction becomes much slower than the rate of lamellar extension, the cell will become elongated and tension will increase between each end of the cell (Fig. 3a, b, d), inhibiting lamellar extension[20] and reducing overall cell speed. When cytoskeletal tension exceeds a critical threshold, stretch-activated calcium channels are activated, triggering an influx of extracellular calcium and a subsequent release of calcium from intracellular stores, which is typical of other mechanochemical signal-transduction systems[21–23]. The transient increase in $[Ca^{2+}]_i$ can then activate various detachment mechanisms that lead to retraction of the cell rear. Possible calcium-dependent detachment mechanisms include: an increased actomyosin-based contractile force[3,24] to pull up the rear cell edge; the disassembly of cell–substratum adhesions by calcium-dependent phosphatases[25]; and proteases[26,27] acting independently or in combination with increased cytoskeletal tension[9,28]. Cytoskeletal tension is decreased after retraction (Fig. 4c, d), removing inhibition of lamellar extension so cell movement can resume.

The activation of stretch-activated calcium channels might account for the spatial[28] and temporal[29] changes in $[Ca^{2+}]_i$ observed in other moving cell types. Thus the function of stretch-activated calcium channels could represent a general mechanism by which cell movement is regulated. □

Methods

Cell culture. Keratocytes from molly fish (*Poecillia sphenops*) or goldfish (*Carassius auratus*) were cultured on coverslips as described[14]. In stretching experiments, cells were dissociated and replated on elastic substrata as described[13].

Bead loading. Dextran-conjugated (relative molecular mass, 10,000) calcium indicator Calcium Green I or a calcium-insensitive rhodamine dextran was incorporated into keratocytes as described[30].

Calibration of the calcium indicator. The calcium indicator was calibrated using the Calcium Calibration kit (#1) from Molecular Probes. The variability of calcium indicator concentration was assessed by loading Calcium Green I dextran with a calcium-insensitive rhodamine-labelled dextran of comparable molecular size (M_r = 10,000). The ratio of Calcium Green I to rhodamine fluorescence was similar in the 20 cells measured, independent of the amount of indicator loaded into the cell, indicating that the resting level of $[Ca^{2+}]_i$ is similar in different cells. To estimate the range of $[Ca^{2+}]_i$ increases, calcium

calibration experiments were performed in about 10 individual cells that had been coloaded with both rhodamine and Calcium Green I, following the observation of 1–2 transients.

Calcium imaging. Cell preparation and calcium imaging were performed as described[30]. Cells attached to coverslips were placed in the well of a metal slide chamber filled with ~0.5 ml of either PBS (with calcium and magnesium) or Fish Ringer solution (containing (in mM): 112 NaCl, 2 KCl, 2.4 NaHCO3, 1 CaCl2, 0.5 MgCl2, 1 TrisCl, pH 7.3. Images were acquired and processed using an intensified CCD camera (MTI 72CCD) in manual mode, and Image 1 software, respectively. Relative changes in fluorescence intensity of the calcium indicator were measured over the nuclear region because the signal-to-noise ratio is higher in this area than in lamellar regions. Camera settings, contrast and brightness settings of Image 1 were the same as for the calibration experiments. Fluorescence images were pseudocoloured for easier observation of calcium transients.

Photoactivation. Photolysis of caged compounds was performed as described[30]. Caged calcium ionophore was used at a final concentration of ~10 μM. Caged inositol 1,4,5-trisphosphate was from Calbiochem-Novabiochem (La Jolla), and the caged calcium ionophore A23187 was synthesized by Molecular Probes.

Cell stretching. Elastic substrata were made as described[13] using the silicone elastomer Sylgard 184 (Dow Corning). Cells previously loaded with calcium indicator were replated onto the elastic substratum. Using a pair of Narashige micromanipulators, glass microneedles were lowered down either side of a cell until they just touched the substratum. With one microneedle held stationary, the other was used to pull the substratum in the opposite direction for 1–2 s. Deformation of cell shape in the direction of the microneedle movement confirmed that the cell had been stretched.

Patch clamping. Cells attached to 12-mm^2 glass coverslips were placed in a glass-bottomed superfusion chamber containing a solution containing (in mM) 145 NaCl, 5 KCl, 2 $CaCl_2$, 1 $MgCl_2$, 10 HEPES, 10 glucose (pH 7.4) situated on the stage of an inverted microscope (Nikon Diaphot). Cells were viewed at a magnification of ×400 using Hoffman modulation contrast optics. Patch pipettes were filled with a standard solution containing (in mM) 150 KCl, 2 $MgCl_2$, 10 HEPES. Cell-attached membrane patches were isolated by forming gigaohm seals (>20 GΩ) using fire-polished glass (Drummond N51A) pipettes with tip openings of ~1 μm diameter and electrical resistance of 2–4 MΩ. Currents were measured with an Axopatch 1C amplifier and continuously logged onto a computer hard disk using Axotape software and a Digidata 1200 interface. Single stretch-activated channels were identified by their activation upon application of negative pressure to the patch pipette and subsequent deactivation upon return to atmospheric pressure. Patch recordings usually lasted less than 2 min because of the rapid movement of keratocytes. In the whole-cell patch-clamp configuration, stretch-activated channels were activated by brief puffs of pressure (1–2 s) applied by mouth through the patch pipette, and channel current was monitored by applying a 200-ms voltage ramp from −110 to +10 mV every 500 ms. Currents were recorded with an EPS-9 amplifier (HEKA), digitized and filtered at 5 kHz (4-pole Bessel) and analysed using Pulsefit and Microsoft Excel. Stretch-activated channel current–voltage relations were obtained by subtracting current measured at each potential in the absence of pipette pressure from that recorded with pressure. Patch pipettes with tip diameters of 3–4 μm (2 MΩ) were pulled from Fisher 50-μl capillary glass, fire polished and filled with an internal saline containing (in mM) 140 aspartate, 10 EGTA, 1 $CaCl_2$, 1 $MgCl_2$, 10 HEPES (pH 7.3 with CsOH). Control external saline contained 145 NaCl, 5 KCl, 2 $CaCl_2$, 1 $MgCl_2$, 10 HEPES (pH 7.4 with NaOH). Calcium saline contained 127 $CaCl_2$, 1 $MgCl_2$ 10 HEPES (pH 7.4 with TrisOH). Gd^{3+} (100 μM) was applied to the bath from a 6X stock in control saline.

Received 16 March; accepted 26 May 1999.

1. Stossel, T P. On the crawling of animal cells. *Science* **260,** 1086–1094 (1993).
2. Strohmeier, R. & Bereiter-Hahn, J. Control of cell shape and locomotion by external calcium. *Exp. Cell Res.* **154,** 412–420 (1984).
3. Citi, S. & Kendrick-Jones, J. Regulations of non-muscle myosin structure and function. *BioEssays* **7,** 155–159 (1987).
4. Rees, D. A. *et al*. Myosin regulation and calcium transients in fibroblast shape change: Attachment and patching. *Cell Motil. Cytoskel.* **13,** 112–122 (1989).
5. Condeelis, J. Life at the leading edge: The formation of cell protrusions. *Annu. Rev. Cell Biol.* **9,** 411–444 (1993).
6. Hartwig, J. H. & Yin, H. The organization and regulation of the macrophage actin skeleton. *Cell Motil. Cytoskel.* **10,** 117–125 (1988).
7. Sjaastad, M. D. & Nelson, W. J. Integrin-mediated calcium signaling and regulation of cell adhesion by intracellular calcium. *BioEssays* **19,** 47–55 (1997).
8. Crowley, E. & Horwitz, A. F. Tyrosine phosphorylation and cytoskeletal tension regulate the release of fibroblast adhesions. *J. Cell Biol.* **131,** 525–537 (1995).
9. Lee, J. & Jacobson, K. The composition and dynamics of cell-substratum adhesions in locomoting fish keratocytes. *J. Cell Sci.* **110,** 2833–2844 (1997).
10. Svitkina, T. M., Verkhovsky, A. B., McQuade, K. M. & Borisy, G. G. Analysis of the actin-myosin II system in fish epidermal keratocytes: Mechanism of cell body translocation. *J. Cell Biol.* **139,** 397–415 (1997).
11. Galbraith, C G. & Sheetz, M. P. Relationship between cell shape, traction force, and speed. *Mol. Biol. Cell* (suppl.) **8,** 385 (1997).
12. Anderson, K. I., Wang, Y.-L. & Small, J. V. Coordination of protrusion and translocation of the keratocyte involves rolling of the cell body. *J. Cell Biol.* **134,** 1209–1218 (1996).
13. Lee, J., Leonard, M., Oliver, T., Ishihara, A. & Jacobson, K. Traction forces generated by locomoting keratocytes. *J. Cell Biol.* **127,** 1957–1964 (1994).
14. Lee, J., Ishihara, A., Theriot, J. A. & Jacobson, K. Principles of locomotion for simple-shaped cells. *Nature* **362,** 167–171 (1993).
15. Theriot, J. A. & Mitchison, T. J. Actin microfilament dynamics in locomoting cells. *Nature* **352,** 126–131 (1991).
16. Sachs, F. in *Sensory Transduction* (eds Corey, D P. & Roper, S.) 242–260 (Rockefeller University Press, New York, 1992).
17. Gustin, M. C., Zhou, X., Martinac, B. & Kung, C. A mechanosensitive ion channel in the yeast plasma membrane. *Science* **242,** 762–765 (1988).
18. Hamill, O. P. & McBride, D. W. Rapid adaptation of single mechanosensitive channels in *Xenopus* oocytes. *Proc. Natl Acad. Sci. USA* **89,** 7462–7466 (1992).
19. Sackin, H. in *Molecular Biology of Membrane Transport Disorders* (ed. Schultz, S. G.) 201–222 (Plenum, New York, 1996).
20. Kolega, J. Effects of mechanical tension on protrusive activity and microfilament and intermediate filament organization in an epidermal epithelium moving in culture. *J. Cell Biol.* **102,** 1400–1411 (1986).
21. Pommerenke, H. *et al*. Stimulation of integrin receptors using a magnetic drag force device induces an intracellular free calcium response. *Eur. J. Cell Biol.* **70,** 157–164 (1996).
22. Glogauer, M., Ferrier, J. & McCulloch, C. A. G. Magnetic fields applied to collagen-coated ferric oxide beads induce stretch-activated Ca^{2+} flux in human fibroblasts. *Am. J. Physiol.* **269,** C1093–C1104 (1995).
23. Naruse, K. & Sokabe, M. Involvement of stretch-activated ion channels in Ca^{2+} mobilization to mechanical stretch in endothelial cells. *Am. J. Physiol.* **264,** 1037–1044 (1993).
24. Chen, W.-T. Mechanism of retraction of the trailing edge during fibroblast movement. *J. Cell Biol.* **90,** 187–200 (1981).
25. Hendey, B., Klee, C. B. & Maxfield, F. R. Inhibition of neutrophil chemokinesis on vitronectin by inhibitors of calcineurin. *Science* **258,** 296–299 (1992).
26. Huttenlocher, A. *et al*. Regulation of cell migration by the calcium-dependent protease calpain. *J. Biol. Chem.* **272,** 32719–32722 (1997).
27. Palecek, S. P., Huttenlocher, A., Horwitz, A. F. & Lauffenburger, D. A. Physical and biochemical regulation of integrin release during rear detachment of migrating cells. *J. Cell Sci.* **111,** 929–940 (1998).
28. Brundage, R. A., Fogarty, K. E., Tuft, R. A. & Fay, F. S. Calcium gradients underlying polarization and chemotaxis of eosinophils. *Science* **254,** 703–706 (1991).
29. Marks, P. W. & Maxfield, F. R. Transient increases in cytosolic free calcium appear to be required for the migration of adherent human neutrophils. *J. Cell Biol.* **110,** 43–52 (1990).
30. Ishihara, A., Gee, K., Schwartz, S., Jacobson, K. & Lee, J. Photoactivation of caged compounds in single, living cells: An application to the study of cell locomotion. *Biotechniques* **23,** 268–274 (1997).

Acknowledgements. This work was supported by the NIH (K.J. and G.O.).

Correspondence and requests for materials should be addressed to J.L. (e-mail: jlee@uconnvm.uconn.edu).